Inorg. Chem. **2003**, *42*, 7887–7896

Mono- and Dinuclear Ruthenium Carbonyl Complexes with Redox-Active Dioxolene Ligands: Electrochemical and Spectroscopic Studies and the Properties of the Mixed-Valence Complexes

Andrew P. Meacham,[†] Kathryn L. Druce,[†] Zöe R. Bell,[†] Michael D. Ward,*[,†,‡] Jerome B. Keister,*[,§] and A. B. P. Lever*[,∥]

School of Chemistry, University of Bristol, Cantock's Close, Bristol BS8 1TS, U.K., Department of Chemistry, University at Buffalo, State University of New York, Buffalo, New York 14260, and Department of Chemistry, York University, 4700 Keele Street, Toronto, Ontario, M3J 1P3, Canada

Received May 28, 2003

The mononuclear complex $[Ru(PPh_3)_2(CO)_2(L^1)]$ (**1**; H_2L^1 = 7,8-dihydroxy-6-methoxycoumarin) and the dinuclear complexes $[\{Ru(PPh_3)_2(CO)_2\}_2(L^2)][PF_6]$ {[**2**][PF_6]; H_3L^2 = 9-phenyl-2,3,7-trihydroxy-6-fluorone} and $[\{Ru(PBu_3)_2(CO)_2\}_2(L^3)]$ (**3**; H_4L^3 = 1,2,3,5,6,7-hexahydroxyanthracene-9,10-dione) have been prepared; all complexes contain one or two *trans*,*cis*-$\{Ru(PR_3)_2(CO)_2\}$ units, each connected to a chelating dioxolene-type ligand. In all cases the dioxolene ligands exhibit reversible redox activity, and accordingly the complexes were studied by electrochemistry and UV/vis/NIR, IR, and EPR spectroscopy in their accessible oxidation states. Oxidation of **1** to [**1**]$^+$ generates a ligand-centered semiquinone radical with some metal character as shown by the IR and EPR spectra. Dinuclear complexes [**2**]$^+$ and **3** show two reversible ligand-centered couples (one associated with each dioxolene terminus) which are separated by 690 and 440 mV, respectively. This indicates that the mixed-valence species [**2**]$^{2+}$ has greater degree of electronic delocalization between the ligand termini than does [**3**]$^+$, an observation which was supported by IR, EPR, and UV/vis/NIR spectroelectrochemistry. Both [**2**]$^{2+}$ and [**3**]$^+$ have a solution EPR spectrum consistent with full delocalization of the unpaired electron between the ligand termini on the EPR time scale (a quintet arising from equal coupling to all four ^{31}P nuclei); [**3**]$^+$ is localized on the faster IR time scale (four CO vibrations rather than two, indicative of inequivalent $\{Ru(CO)_2\}$ units) whereas [**2**]$^{2+}$ is fully delocalized (two CO vibrations). UV/vis/NIR spectroelectrochemistry revealed the presence of a narrow, low-energy (2695 nm) transition for [**3**]$^+$ associated with the catecholate → semiquinone intervalence transition. The narrowness and solvent-independence of this transition (characteristic of class III mixed-valence character) coupled with evidence for inequivalent $\{Ru(CO)_2\}$ termini in the mixed-valence state (characteristic of class II character) place this complex at the class II–III borderline, in contrast to [**2**]$^{2+}$ which is clearly class III.

Introduction

Chelating 1,2-dioxolenes[1] have attracted much attention as ligands recently, in part because of their noninnocent behavior[2] which can lead to unusual properties for their complexes. The presence of ligand-based redox activity in the complexes—as exemplified by the catecholate (cat)/semiquinone (sq)/quinone (q) redox series—combined with, in many cases, metal-based redox activity means that dioxolene complexes can have exceptionally rich redox and spectroscopic behavior. For example, in Pierpont's "redox isomers" based on first-row transition-metal complexes, the proximity of metal-based and ligand-based redox orbitals

* Authors to whom correspondence should be addressed. Fax: (+44) 117 9290509 (M.D.W.). E-mail: m.d.ward@sheffield.ac.uk (M.D.W.); blever@yorku.ca (A.B.P.L.); keister@buffalo.edu (J.B.K.).
† University of Bristol.
‡ Present address: Department of Chemistry, University of Sheffield, Sheffield, U.K., S3 7HF.
§ University of Buffalo.
∥ University of York.

(1) Pierpont, C. G.; Lange, C. W. *Prog. Inorg. Chem.* **1994**, *41*, 331.

(2) Ward, M. D.; McCleverty, J. A. *J. Chem. Soc., Dalton Trans.* **2002**, 275.

10.1021/ic034579o CCC: $25.00
Published on Web 11/05/2003

Scheme 1. Structural Formulas of the New Complexes

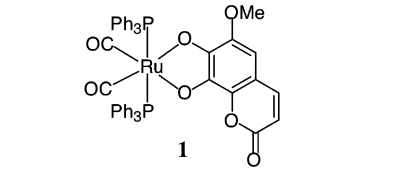

1

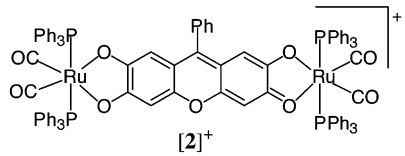

[**2**]$^+$

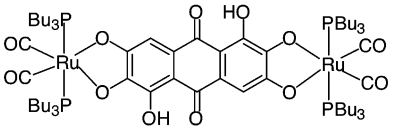

3

allows for an unusual type of switching behavior.[3] In addition, complexes of dioxolenes containing Ru(II) or Os(II) termini with polypyridine or ammine coligands have been subjected to extensive theoretical and spectroscopic studies which have provided insights into the charge distribution;[4] many of these complexes also show pronounced near-IR electrochromism arising from metal-to-dioxolene charge-transfer transitions.[5]

In this paper we describe the synthesis, redox, and spectroelectrochemical properties of some organometallic ruthenium complexes containing $\{Ru(PR_3)_2(CO)_2\}$ units attached to mononucleating and bridging dioxolene ligands, as shown in Scheme 1. Mononuclear complex **1** is based on 7,8-dihydroxy-6-methoxycoumarin (H_2L^1), dinuclear complex [**2**][PF_6] is based on 9-phenyl-2,3,7-trihydroxy-6-fluorone (H_3L^2), and dinuclear complex **3** is based on 1,2,3,5,6,7-hexahydroxyanthracene-9,10-dione (H_4L^3, also known as rufigallol). A variety of mononuclear complexes of the type $[Ru(PR_3)_2(CO)_2(OO)]$ (where "OO" denotes a generic catecholate-type ligand) have been investigated, and show reversible ligand-centered redox activity;[6,7] we are now extending this area to the study of dinuclear analogues. In complexes of $[L^2]^{3-}$ and $[L^3]^{4-}$, which have two dioxolene-like termini, redox processes associated with each terminus are expected to lead to extensive ligand-centered redox activity. Further, the combination of intense colors and multiple oxidation states suggests the possibility of using the complexes as switchable dyes.

Although examples of dinuclear complexes with bis-dioxolene bridging ligands based on $\{Ru(bpy)_2\}^{2+}$ and $\{Os(bpy)_2\}^{2+}$ termini are known,[5] organometallic analogues of the type we describe here have received scant attention. Inclusion of the CO and phosphine units (instead of, for example, bpy units) as coligands facilitates the spectroscopic studies of the complexes in their different oxidation states. The CO stretches in the IR spectra provide a convenient method for assessing changes in electron density at each metal center by IR spectroelectrochemistry, and the spin-active ^{31}P nuclei result in simple hyperfine coupling patterns in the EPR spectra of the paramagnetic oxidation states which also affords useful information. Accordingly we describe here IR, EPR, and UV/vis/NIR spectroelectrochemical studies on the complexes which provide an interesting picture of how the different structures of the dinucleating bridging ligands $[L^2]^{3-}$ and $[L^3]^{4-}$ result in different electron-delocalization properties in their mixed-valence states.

Results and Discussion

Synthesis and Characterization. The complexes were readily prepared by reaction of $Ru_3(CO)_{12}$, the appropriate phosphine, and the dioxolene ligand in refluxing toluene which afforded a deeply colored solution in each case. Complexes **1** and **3** are neutral and were isolated by chromatography of the crude reaction mixture; complex [**2**]-[PF_6] is a monocation (due to the presence of only three dissociable protons in H_3L^2) and was accordingly isolated as its hexafluorophosphate salt. In all cases, two CO stretches were observed in the IR spectrum, confirming their mutual cis orientation in approximate local C_{2v} symmetry. A single signal in the ^{31}P NMR spectrum in every case is also consistent with the *trans*-$(PR_3)_2$, *cis*-$(CO)_2$ arrangement of ancillary ligands which occurs in other mononuclear complexes of this type.[7] The formulations of the complexes were further confirmed by mass spectrometry and elemental analyses. Although complex [**2**][PF_6] appears to be asymmetric, with inequivalent dioxolene-like binding sites (carrying 2− and 1− charges), the picture in Scheme 1 represents only one extreme canonical form and delocalization renders the two termini equivalent,[5c] as shown by the NMR and IR spectra. Complex **3** was easily characterized by comparison of spectroscopic data to the 1,2,3-trihydroxyanthraquinone monometallic analogue;[6a] an alternative 1,2- and 5,6-complex geometry can be excluded because of the low-field shift of the hydroxyl resonance, which indicates hydrogen-bonding to the central quinone carbonyl.

(3) (a) Pierpont, C. G. *Inorg. Chem.* **2001**, *40*, 5727. (b) Pierpont, C. G. *Coord. Chem. Rev.* **2001**, *219*, 415. (c) Pierpont, C. G. *Coord. Chem. Rev.* **2001**, *216*, 99. (d) Attia, A. S.; Pierpont, C. G. *Inorg. Chem.* **1998**, *37*, 3051. (e) Jung, O. S.; Jo, D. H.; Lee, Y. A.; Conklin, B. J.; Pierpont, C. G. *Inorg. Chem.* **1997**, *36*, 19.

(4) (a) Gorelsky, S. I.; Dodsworth, E. S.; Lever, A. B. P.; Vlcek, A. A. *Coord. Chem. Rev.* **1988**, *174*, 469. (b) da Silva, R. S.; Gorelsky, S. I.; Dodsworth, E. S.; Tfouni, E.; Lever, A. B. P. *J. Chem. Soc., Dalton Trans.* **2000**, 4078. (c) Lever, A. B. P.; Masui, H.; Metcalfe, R. A.; Stufkens, D. J.; Dodsworth, E. S.; Auburn, P. R, *Coord. Chem. Rev.* **1993**, *125*, 317. (d) Venegas-Yazigi, D.; Mirza, H.; Lever, A. B. P.; Lough, A. J.; Costamanga, J.; Vega, A.; LaTorre, R. *Inorg. Chem.* **2000**, *39*, 141.

(5) (a) Joulié, L. F.; Schatz, E.; Ward, M. D.; Weber, F.; Yellowlees, L. J. *J. Chem. Soc., Dalton Trans.* **1994**, 799. (b) Barthram, A. M.; Cleary, R. L.; Kowallick, R.; Ward, M. D. *Chem. Commun.* **1998**, 2695. (c) Barthram, A. M.; Ward, M. D. *New J. Chem.* **2000**, *24*, 501. (d) Barthram, A. M.; Reeves, Z. R.; Jeffery, J. C.; Ward, M. D. *J. Chem. Soc., Dalton Trans.* **2000**, 3162.

(6) (a) Churchill, M. R.; Keil, K. M.; Gilmartin, B. P.; Schuster, J. J.; Keister, J. B.; Janik, T. S. *Inorg. Chem.* **2001**, *40*, 4361. (b) Churchill, M. R.; Keil, K. M.; Bright, F. V.; Pandey, S.; Baker, G. A.; Keister, J. B. *Inorg. Chem.* **2000**, *39*, 5807.

(7) (a) Connelly, N. G.; Manners, I.; Protheroe, J. R. C.; Whiteley, M. W. *J. Chem. Soc., Dalton Trans.* **1984,** 2713. (b) Girgis, A. Y.; Sohn, Y. S.; Balch, A. L. *Inorg. Chem.* **1975**, *14*, 2327.

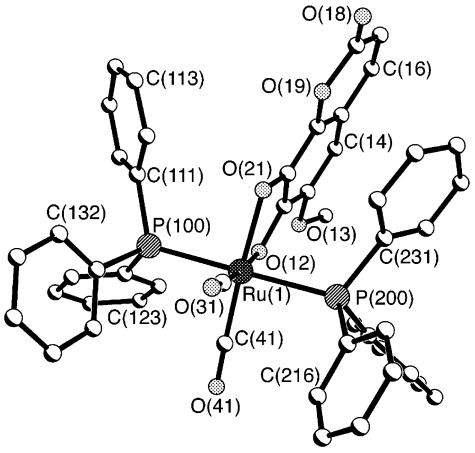

Figure 1. Structure of complex **1**.

The crystal structures of complexes **1** and [**2**][PF_6]·3CH_2Cl_2 have been determined; see Figures 1 and 2 and Tables 1−3. For **1** (Figure 1), the *trans*-(PR_3)$_2$, *cis*-(CO)$_2$ arrangement of ligands is apparent, and the O(12)−C(12) and O(21)−C(21) separations of 1.34 Å each are in agreement with a fully reduced catecholate ligand coordinated to a Ru(II) center.[8]

In the structure of complex [**2**][PF_6]·3CH_2Cl_2, the coordination environment around each of the metal centers of the complex cation is essentially the same as in **1** (compare Tables 2 and 3). One significant difference, however, is that the C−O distances in the bridging ligand associated with the four donor atoms O(11), O(24), O(17), and O(18) are uniformly shorter in [**2**]$^+$ (average, 1.302 Å) than the corresponding C−O distances in **1** (1.34 Å). This arises from the partial double bond character due to the presence of (formally) one double and three single C−O bonds which are rendered equivalent by delocalization; there is no localization of single and double C−O bonds on the basis of the structural data. There is disorder in the bridging ligand involving the position of the phenyl substituent [C(141)−C(146)] and the oxygen atom O(21) which is discussed in more detail in the Experimental Section.

Electrochemical Studies. The cyclic voltammogram of **1** in CH_2Cl_2 (see Table 4) showed a reversible, one-electron couple at −0.17 V vs ferrocenium/ferrocene and a second process at +0.86 V which is irreversible (the return wave is of lower intensity than the outward wave, and there is a small product wave at +0.52 V). Square-wave voltammetry showed the two processes to be of equal intensity, and by analogy with the behavior of previously described complexes of this nature,[7] these are assigned as successive cat/sq and sq/q processes centered on the dioxolene ligand; the separation of about 1 V between the two couples and the irreversibility of the second couple are both characteristic of complexes of this type, as are the redox potentials.[7]

The dinuclear complex [**2**][PF_6] displayed under the same conditions two reversible one-electron couples at +0.07 and +0.76 V vs ferrocene/ferrocenium. A third process at +1.52 V, near the limit of the solvent window, was detected by square-wave voltammetry, but it did not appear to be reversible by cyclic voltammetry. Again, we assign these as ligand-centered, with the first two being analogous to the cat/sq couple of **1,** with one being associated with each binding site. It is perhaps not strictly accurate to call these "cat/sq" processes, since the binding sites in [**2**]$^+$ are not wholly catecholate-like in that they carry a charge of −1.5 (rather than −2) and have a formal C−O bond order of greater than 1 due to the contribution of a single C═O component (Scheme 1). However [L^2]$^{3-}$ may be considered as catecholate-like because it is in its fully reduced, diamagnetic form, with the two reversible processes resulting first in a semiquinone-like ligand radical species, and then a diamagnetic quinone-like form (Scheme 2). The third couple we assume to be also ligand-centered; the related complex [{Ru(bpy)$_2$}$_2$(μ−L^2)]$^+$ also underwent three ligand-centered redox processes which were all chemically reversible.[5c] An important question relating to complex [**2**]$^+$ is whether the mono-oxidized radical form [**2**]$^{2+}$, which may be considered as a ligand-centered mixed-valence species, is fully delocalized (resulting in equivalent Ru centers) or is localized (resulting in spectroscopically distinct Ru centers); this will be addressed later. The separation of 690 mV between the first two redox processes means that the comproportionation constant for the mixed-valence state, K_c, is 7×10^{11}, which is in the domain indicative of strongly interacting, class III (fully delocalized) mixed-valence states.[9]

In complex **3** the two binding termini of the bridging ligand are catecholate-like units, and accordingly (by analogy with **1**) we may expect a reversible cat/sq couple and an irreversible sq/q couple associated with each of the two metal−dioxolene fragments. In CH_2Cl_2 the cyclic voltammogram shows two reversible one-electron processes at −0.07 and +0.37 V vs ferrocene/ferrocenium, which we assign as cat/sq couples associated with the two Ru−catecholate substructures (the two sq/q couples are not apparent, presumably occurring at potentials beyond the limit of the solvent). The separation of 440 mV between these couples indicates a strong electronic interaction between the two sites (K_c for the mixed-valence state is 4×10^7), although the interaction is significantly weaker than that observed in complex [**2**]$^+$, indicative of a reduced degree of delocalization of the unpaired electron in the mixed-valence state of **3**.

IR and EPR Studies. The IR and EPR spectroscopic properties of **1** in its neutral and oxidized forms provide a useful reference for comparison with the mixed-valence dinuclear complexes [**2**]$^{2+}$ and [**3**]$^+$. Complex **1** could be oxidized to [**1**]$^+$, either chemically (using ferrocenium hexafluorophosphate) or electrochemically (in a KBr OTTLE cell). On oxidation, the two CO stretching vibrations of the carbonyl ligands, which start at 1978 and 2042 cm^{-1}, move to 2018 and 2072 cm^{-1} respectively, an average shift of 35 cm^{-1} to higher energy which is consistent with a slight

(8) (a) Pierpont, C. G.; Buchanan, R. M. *Coord. Chem. Rev.* **1981**, *38*, 45. (b) Haga, M.; Dodsworth, E. S.; Lever, A. B. P.; Boone, S. R.; Pierpont, C. G. *J. Am. Chem. Soc.* **1986**, *108*, 7413. (c) Boone, S. R.; Pierpont, C. G. *Inorg. Chem.* **1987**, *26*, 1796. (d) Haga, M.; Isobe, K.; Boone, S. R.; Pierpont, C. G. *Inorg. Chem.* **1990**, *29*, 3795.

(9) (a) Ward, M. D. *Chem. Soc. Rev.* **1995**, 121. (b) Creutz, C. *Prog. Inorg. Chem.* **1983**, *30*, 1. (c) Hush, N. S. *Coord. Chem. Rev.* **1985**, *64*, 135.

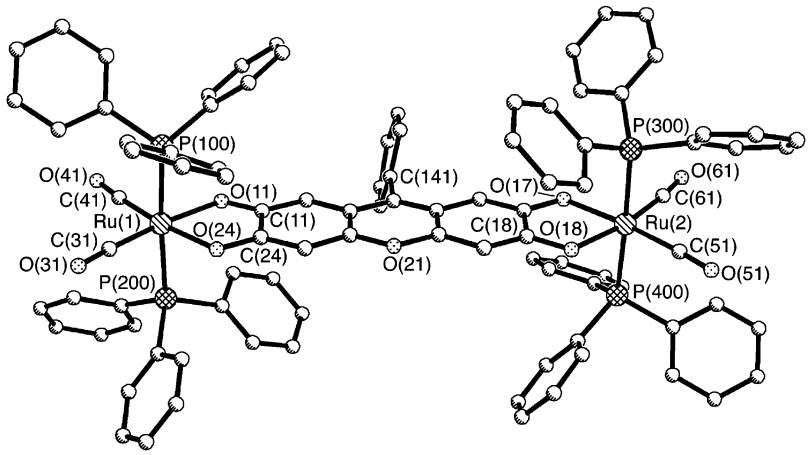

Figure 2. Structure of the complex cation of $[\mathbf{2}][PF_6]\cdot 3CH_2Cl_2$.

Table 1. Crystallographic Data for Complexes **1** and $[\mathbf{2}][PF_6]\cdot 3CH_2Cl_2$

complex	**1**	$[\mathbf{2}][PF_6\cdot 3CH_2Cl_2$
empirical formula	$C_{48}H_{36}O_7P_2Ru_2$	$C_{98}H_{75}Cl_6F_6O_9P_5Ru_2$
fw	887.78	2080.27
wavelength, Å	0.71073	0.71073
space group	$P\bar{1}$	$P\bar{1}$
a, Å	12.0966	14.380(4)
b, Å	13.2288	16.759(5)
c, Å	15.691	21.153(8)
α, deg	103.585(11)	85.70(3)
β, deg	90.756(15)	87.55(2)
γ, deg	116.967(8)	74.64(2)
vol, Å^3	2154.4(5)	4901(3)
Z	2	2
calcd density, Mg/m^3	1.369	1.410
μ(mm^{-1})	0.488	0.619
final *R* indices	R1 = 0.0261	0.0603
[$I > 2\sigma(I)$]	wR2 = 0.0558	0.1305
final *R* indices	R1 = 0.0392	0.1078
(all data)	wR2 = 0.0580	0.1467

Table 2. Selected Bond Lengths (Å) and Angles (deg) for **1**

Ru(1)−C(41)	1.8737(18)	Ru(1)−O(21)	2.0722(11)
Ru(1)−C(31)	1.8840(l9)	Ru(1)−P(100)	2.4009(6)
Ru(1)−O(12)	2.0528(12)	Ru(1)−P(200)	2.4297(6)
C(12)−O(12)	1.343(2)	C(21)−O(21)	1.3438(19)
C(18)−O(18)	1.213(2)	C(18)−O(19)	1.380(2)

C(41)−Ru(1)−C(31)	93.31(7)	C(41)−Ru(1)−O(12)	92.90(6)
C(31)−Ru(1)−O(12)	173.72(6)	C(41)−Ru(1)−O(21)	174.04(6)
C(31)−Ru(1)−O(21)	92.34(6)	O(12)−Ru(l)−O(21)	81.48(4)
C(41)−Ru(1)−P(100)	89.88(6)	C(31)−Ru(1)−P(100)	91.94(6)
O(12)−Ru(1)−P(100)	87.18(4)	O(21)−Ru(1)−P(100)	91.82(4)
C(41)−Ru(1)−P(200)	90.49(6)	C(31)−Ru(1)−P(200)	89.64(6)
O(12)−Ru(1)−P(200)	91.19(4)	O(21)−Ru(1)−P(200)	87.66(4)
P(100)−Ru(1)−P(200)	178.347(18)		

Table 3. Selected Bond Lengths (Å) and Angles (deg) for $[\mathbf{2}][PF_6]\cdot 3CH_2Cl_2$

Ru(1)−C(31)	1.868(6)	Ru(2)−C(61)	1.878(6)
Ru(1)−C(41)	1.874(6)	Ru(2)−C(51)	1.881(7)
Ru(1)−O(11)	2.062(4)	Ru(2)−O(17)	2.065(3)
Ru(1)−O(24)	2.074(3)	Ru(2)−O(18)	2.073(3)
Ru(1)−P(100)	2.4150(17)	Ru(2)−P(400)	2.4016(17)
Ru(1)−P(200)	2.4163(17)	Ru(2)−P(300)	2.4076(17)
O(11)−C(11)	1.289(7)	O(18)−C(18)	1.310(6)
O(24)−C(24)	1.305(6)	O(17)−C(17)	1.305(6)

C(31)−Ru(1)−C(41)	95.2(2)	C(61)−Ru(2)−C(51)	96.0(2)
C(31)−Ru(1)−O(11)	172.3(2)	C(61)−Ru(2)−O(17)	90.31(19)
C(41)−Ru(1)−O(11)	92.5(2)	C(51)−Ru(2)−O(17)	173.7(2)
C(31)−Ru(1)−O(24)	92.10(19)	C(61)−Ru(2)−O(18)	169.9(2)
C(41)−Ru(1)−O(24)	172.6(2)	C(51)−Ru(2)−O(18)	93.9(2)
O(11)−Ru(1)−O(24)	80.18(14)	O(17)−Ru(2)−O(18)	79.82(14)
C(31)−Ru(1)−P(100)	90.76(17)	C(61)−Ru(2)−P(400)	91.34(17)
C(41)−Ru(1)−P(100)	91.65(17)	C(51)−Ru(2)−P(400)	91.47(17)
O(11)−Ru(1)−P(100)	88.91(11)	O(17)−Ru(2)−P(400)	87.87(11)
O(24)−Ru(1)−P(100)	87.24(11)	O(18)−Ru(2)−P(400)	90.35(11)
C(31)−Ru(1)−P(200)	91.28(17)	C(61)−Ru(2)−P(300)	90.42(17)
C(41)−Ru(1)−P(200)	91.73(17)	C(51)−Ru(2)−P(300)	89.74(17)
O(11)−Ru(1)−P(200)	88.59(11)	O(17)−Ru(2)−P(300)	90.73(11)
O(24)−Ru(1)−P(200)	89.10(11)	O(18)−Ru(2)−P(300)	87.68(11)
P(100)−Ru(1)−P(200)	175.88(5)	P(400)−Ru(2)−P(300)	177.76(5)

Table 4. Electrochemical Data[a]

	redox potentials [$E_{1/2}$, V vs Fc/Fc$^+$]	
complex	A[b]	B[c]
1	−0.17	+0.86
$[\mathbf{2}]^+$	+0.07, +0.76	+1.52
3	−0.07, +0.37	

[a] Measurements made at a Pt-bead working electrode in CH_2Cl_2 containing 0.1 M ^{n}Bu$_4$NPF$_6$ as base electrolyte; scan rate was 0.2 V s^{-1}. [b] Fully reversible catecholate/semiquinone interconversions. [c] Irreversible semiquinone/quinone interconversions.

decrease in electron density at the metal center. This is a relatively small shift, in agreement with the oxidation being a largely ligand-centered cat/sq couple; wholly metal-centered oxidations of carbonyl complexes result in shifts of ca.100 cm^{-1} of the CO stretching vibrations to higher energy.[10,11] In addition, the carbonyl stretching vibration associated with the coumarin ester unit moves from 1686 to 1725 cm^{-1}; oxidation of the catecholate unit to semiquinone decreases its ability to act as an electron-rich substituent to this ester group, and accordingly this ligand-centered CO vibration also moves to higher energy.

The EPR spectrum of chemically generated $[\mathbf{1}]^+$ (Figure 3a) also confirms the substantially ligand-centered nature of the oxidation. The *g* value of 2.0013 is close to that expected for organic radicals, and the hyperfine coupling constants to the metal and phosphine ligands are small. The most obvious feature of the hyperfine coupling is the triplet, which has a coupling constant A_P of 22 G, arising from coupling to two equivalent ^{31}P nuclei. (That this coupling involves

(10) (a) Anderson, K. M.; Connelly, N. G.; Llamas-Rey, E.; Orpen, A. G.; Paul, R. L. *Chem. Commun.* **2001**, 1734. (b) Connelly, N. G.; Hicks, O. M.; Lewis, G. R.; Orpen, A. G.; Wood, A. J. *J. Chem. Soc., Dalton Trans.* **2000**, 1637.
(11) Atwood, C. G.; Geiger, W. E. *J. Am. Chem. Soc.* **2000**, *122*, 5477.

Scheme 2. Sketches of the Oxidized Forms of $[L^2]^{3-}$ and $[L^3]^{4-}$ [a]

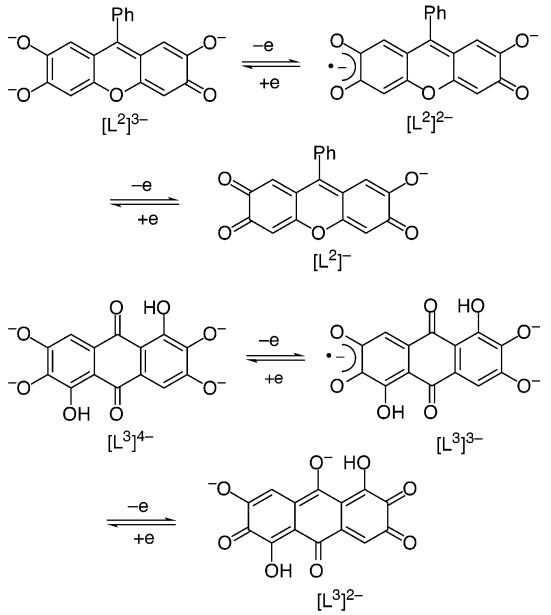

[a] Only one canonical form is represented for each oxidation state.

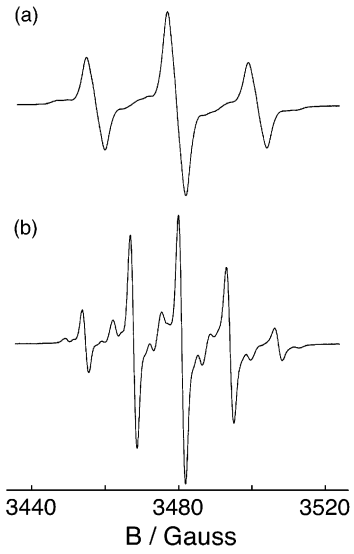

Figure 3. X-band EPR spectra (in CH_2Cl_2) of the ligand-centered radical species (a) $[\mathbf{1}]^+$ and (b) $[\mathbf{2}]^{2+}$ (the EPR spectrum of $[\mathbf{3}]^+$ is very similar to that of $[\mathbf{2}]^{2+}$).

the axial phosphine ligands and not the semiquinone radical H atoms was shown by Connelly et al., who observed a similar EPR spectrum on oxidation of $[Ru(PPh_3)_2(CO)_2(Cl_4cat)]$, which has no H atoms on the dioxolene ligand).[7a] Closer inspection also reveals small satellites on each component of the triplet, which are the outermost lines of the sextet arising from coupling to those spin-active Ru nuclei which have $I = {}^5/_2$, from which a coupling constant A_{Ru} of 4 G can be determined.

Complex **2** was studied by IR spectroelectrochemistry at 243 K in the three accessible oxidation states, with charges of +1, +2 (radical), and +3. The two CO stretching vibrations are at 1988 and 2046 cm^{-1} in $[\mathbf{2}]^+$; on oxidation to $[\mathbf{2}]^{2+}$ they move to 2010 and 2063 cm^{-1}, respectively, an average shift of ca.19 cm^{-1} (Figure 4a). The facts that two

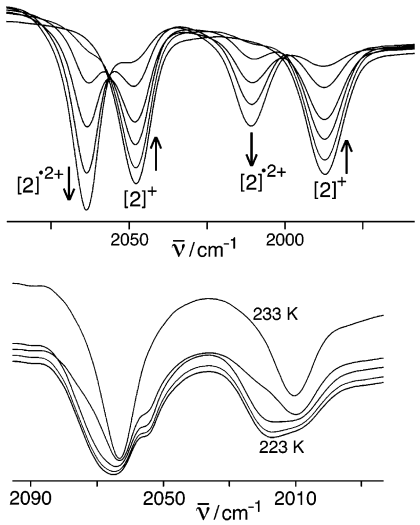

Figure 4. (a, top) IR spectra recorded during oxidation of $[\mathbf{2}]^+$ to $[\mathbf{2}]^{2+}$ in an OTTLE cell (CH_2Cl_2, 243 K). (b, bottom) Temperature dependence of the spectrum of the mixed-valence complex $[\mathbf{2}]^{2+}$ between 233 and 223 K.

CO vibrations are observed in the mixed-valence state, and that the shift from the neutral form is approximately half of that observed following oxidation of **1** to $[\mathbf{1}]^+$, both indicate that the odd electron in $[\mathbf{2}]^{2+}$ is fully delocalized across the bridging ligand at 243 K, resulting in two equivalent termini with the positive charge evenly shared between them on the fast IR time scale. Cooling of the sample, however, resulted in the two peaks becoming four; this occurs between 233 and 223 K, and the spectral changes (Figure 4b) were fully reversible over several heating/cooling cycles. The reduction in temperature is slowing the electron delocalization rate down to the extent where it becomes slow on the IR time scale at 223 K. The spectrum that is observed at 223 K is far from being a fully localized spectrum, in which two CO vibrations would be unshifted (at the same position as in $[\mathbf{2}]^+$) whereas two would be shifted by ca. 30−40 cm^{-1} (cf. the shift observed on oxidation of **1** to $[\mathbf{1}]^+$), but it does show the transition from fully delocalized on the IR time scale at 233 K to the onset of localization by 223 K.

Further oxidation to $[\mathbf{2}]^{3+}$ at 243 K results in a similar further shift to higher energy of the carbonyl peaks, to 2030 and 2076 cm^{-1}, an average shift of an additional 17 cm^{-1}; these values for $[\mathbf{2}]^{3+}$ are quite similar to those seen for $[\mathbf{1}]^+$ because of the presence of one additional positive charge associated with each Ru−dioxolene terminus in each case.

In keeping with the fully delocalized nature of $[\mathbf{2}]^{2+}$ at temperatures above 233 K, as shown by the IR spectra, its isotropic EPR spectrum at room temperature (cf. Figure 3b) shows a quintet at $g = 2.00$ due to hyperfine coupling to four equivalent phosphorus nuclei; given that EPR has a slower time scale than IR (ca. 10^{-8} vs 10^{-13} s), this was to be expected. The coupling constant A_P of 13.5 G is much less than that observed in $[\mathbf{1}]^+$, as is the coupling to the ruthenium nuclei ($A_{Ru} = 1.9$ G), both of which are consistent with the fact that greater delocalization of the electron will reduce the magnitude of its coupling to each spin with which it interacts. To a first approximation, the difference in these coupling constants between a mononuclear complex and an

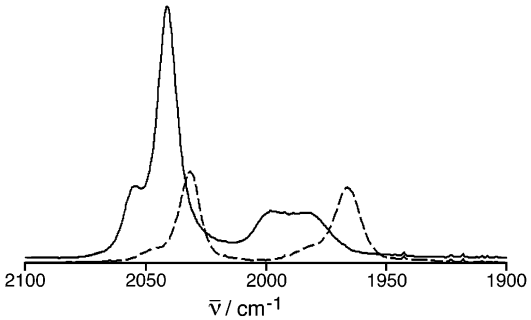

Figure 5. IR spectra of **3** (dashed line) and $[\mathbf{3}]^+$ (solid line) in CH_2Cl_2 at room temperature.

analogous dinuclear complex should be a factor of 2, in reasonable agreement with what we observe.

In complex **3** the two CO stretching vibrations are at 1965 and 2030 cm^{-1} with almost equal intensities. One-electron oxidation, either chemically (ferrocenium hexafluorophosphate) or electrochemically (OTTLE cell) resulted in these being replaced by four new peaks at 2055 (m), 2040 (vs), 1998 (m), and 1980 (m) cm^{-1} (Figure 5). The presence of four peaks indicates that the complex is no longer symmetric, with the oxidation being localized at one terminus more than the other, as observed for $[\mathbf{2}]^{2+}$ below 233 K. However, if the semiquinone site were completely localized at one terminus, we would expect to see—by analogy with the results above—two CO peaks that scarcely move, associated with the catecholate terminus, and two which move by about 35 cm^{-1} on average, associated with the semiquinone terminus. In fact, we see one pair of peaks (1980 and 2040 cm^{-1}) shifted by an average of 12 cm^{-1}, and the other (1998 and 2055 cm^{-1}) shifted by an average of 29 cm^{-1}. Furthermore, the relative intensities of the peaks are unexpected. Complex **3** displays symmetric and antisymmetric stretches of roughly equal intensities, typical of *cis*-$Ru(CO)_2$ fragments with OC−Ru−CO angles ca. 90°; for $[\mathbf{3}]^+$, three of the absorptions are comparable and with slightly lower intensity than for **3**, but the 2040 cm^{-1} band is 4−5 times more intense than the others. This should be a textbook example relating the inter-carbonyl angle to the ratio of intensities of the symmetric and antisymmetric stretches.[12] However, this cannot be the explanation here for the variations in intensities because the OC−Ru−CO angle would have to be unreasonably small. A possible explanation for the greater intensity of the 2040 cm^{-1} band is that the four CO stretches are coupled. Assuming approximate C_{2v} symmetry (not D_{2h} because the metal termini are no longer equivalent), the four CO stretching vectors combine to give a totally symmetric A_1 mode (expected to be of highest frequency), an asymmetric (with respect to the molecular center) A_1 mode (next highest in frequency), and two lower frequency B_1 modes. The asymmetric A_1 mode has the same symmetry as those vibrations in the Ru−(rufigallolate)−Ru plane which would accompany intervalence charge transfer, which might allow for an increase in intensity for this mode alone compared to the other three. Complex $[\mathbf{3}]^+$ is apparently behaving somewhere between completely delocalized and completely localized, indicative of class II behavior, with the rate of electron hopping between the termini in the mixed-valence state being slow on the IR time scale ($<10^{13}$ s^{-1}) at room temperature; this decreased delocalization compared to $[\mathbf{2}]^{2+}$ (which is fully delocalized down to 233 K) is in agreement with the electrochemical data described above. Further oxidation to $[\mathbf{3}]^{2+}$ results in the four CO stretches being replaced by two, at 2012 and 2063 cm^{-1} (cf. the mononuclear semiquinone complex $[\mathbf{1}]^+$), as the complex regains its 2-fold symmetry with each ligand terminus becoming a semiquinone unit.

Since the mixed-valence species $[\mathbf{3}]^+$ is localized on the IR time scale, it was of particular interest to examine this species by EPR spectroscopy to see if the delocalization could be "bracketed" by the different time scales of the two methods. The EPR spectrum of $[\mathbf{3}]^+$ does indeed show a quintet centered at $g = 2.006$, arising from equal coupling to all four ^{31}P nuclei, with $A_P = 12.1$ G and $A_{Ru} = 2$ G. These coupling constants are very similar to those seen for $[\mathbf{2}]^{2+}$ and about half the magnitude of those seen for $[\mathbf{1}]^+$ (the appearance of this spectrum is almost identical to that of $[\mathbf{2}]^{2+}$, Figure 3b). It is clear that the unpaired electron in $[\mathbf{3}]^+$ is delocalized on the EPR time scale despite being localized on the IR time scale, such that its exchange rate between the two dioxolene sites is $>10^8$ s^{-1} but $<10^{13}$ s^{-1} at room temperature. (The same applies to $[\mathbf{2}]^{2+}$ but only at temperatures below 223 K; at higher temperatures it is fully delocalized by both EPR and IR methods.) Similar behavior has been described recently for a mixed-valence dinuclear Mo(I)/Mo(II) complex, where the unpaired electron showed equal coupling to both Mo nuclei in the EPR spectrum, but the IR spectrum showed the presence of two sets of vibrations associated with distinct Mo(I) and Mo(II) termini.[13] Geiger and co-workers have also described how the dinuclear mixed-valence complex $[(fulv)\{Mn(CO)_2\}_2]^+$ (fulv = fulvalenediyl) is delocalized according to EPR spectroscopy but localized according to IR spectroscopy.[11]

UV/Vis/NIR Spectroelectrochemical Studies. All three complexes were examined by UV/vis/NIR spectroelectrochemistry in CH_2Cl_2 using an OTTLE cell thermostated at 243 K; the redox interconversions examined were fully chemically reversible, as shown by the presence of clean isosbestic points during the interconversions in all cases.

(i) Spectra of Mononuclear Complex 1. The spectrum of **1** (Figure 6, Table 5) shows three discernible transitions, with clear absorption maxima at 432 and 279 nm, and a shoulder at about 375 nm. On oxidation to $[\mathbf{1}]^+$ these transitions all change slightly; the transition at ca. 430 nm is diminished in intensity, and new transitions appear at 341, 535, and 582 nm. In addition, at lower energy, a weak transition appears at ca. 1250 nm which is not shown in the figure.

Partial assignments for these electronic spectra can be made on the basis of ZINDO calculations on the complexes,

(12) Cotton, F. A.; Wilkinson, G. *Advanced Inorganic Chemistry*, 5th ed.; Wiley-Interscience: New York, 1988; pp 1035−1037.

(13) Wlodarczyk, A.; Maher, J. P.; McCleverty, J. A.; Ward, M. D. *J. Chem. Soc., Dalton Trans.* **1997**, 3287.

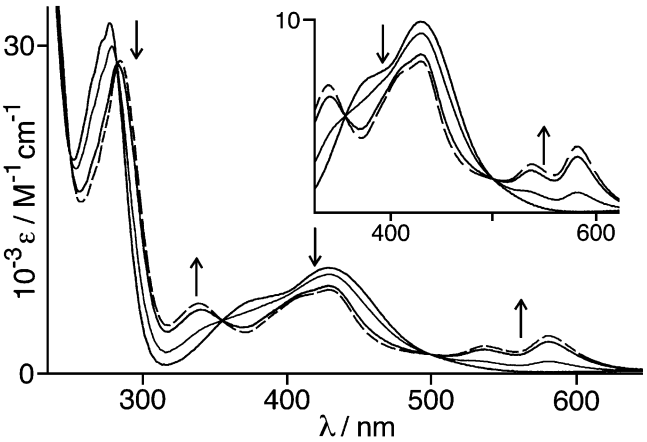

Figure 6. Electronic spectra recorded during oxidation of **1** to $[\mathbf{1}]^+$ in an OTTLE cell (CH_2Cl_2, 243 K; the spectrum of the fully oxidized form is shown as a dashed line for clarity).

Table 5. Results of UV/Vis/NIR and IR Spectroelectrochemical Studies (CH_2Cl_2, 243 K)[a]

complex	ν(CO), cm^{-1}	λ_{max}, nm ($10^{-3}\epsilon$, $dm^3\,mol^{-1}\,cm^{-1}$)
1	1978, 2042	279 (32), 432 (10)
$[\mathbf{1}]^+$	2018, 2072	283 (28), 341 (6.0), 433 (7.9), 535 (2.2), 582 (2.9), ≈1250 (0.2)
$[\mathbf{2}]^+$	1988, 2046	272 (38), 599 (48), 899 (0.4)
$[\mathbf{2}]^{2+}$	2010, 2063	272 (38), 626 (33), 899 (4.8), 1995 (0.2)
$[\mathbf{2}]^{3+}$	2030, 2076	294 (34), 630 (34), 670 (13), 820 (16), 1348 (4.3), 1714 (16)
3	1965, 2030	360 (92), 430 (sh), 449 (14), 547 (10)
$[\mathbf{3}]^+$	2055, 2040, 1998, 1980	288 (18), 342 (12), 398 (39), 464 (13), 556 (6.3), 682 (6.1), 1118 (4.4), 2695 (16)
$[\mathbf{3}]^{2+}$	2012, 2063	294 (18), 521 (10), 802 (11)

[a] Suggested assignments for the electronic spectra are given in the main text.

using the geometry provided by the X-ray structure (for **1**) and the DFT-minimized geometry (for $[\mathbf{1}]^+$). Because of the low symmetry there is extensive orbital mixing and only the dominant contributions are given; a more detailed analysis will be the subject of a future paper. For **1** the HOMO is a π-orbital on the catecholate ligand, with a small admixture of metal d(π) character; the LUMO is a catecholate-centered π^* orbital. The 432 nm transition of **1** is therefore mostly catecholate-centered $\pi \rightarrow \pi^*$ with a small Ru[d(π)] $\rightarrow$ catecholate (π^*) MLCT component. The high-energy shoulder on this, and the more intense transition in the UV region at 279 nm, both consist of a similar mixture of (higher-energy) catecholate-centered $\pi \rightarrow \pi^*$ and Ru[d(π)] $\rightarrow$ catecholate (π^*) transitions, with the former dominating.

For the oxidized complex $[\mathbf{1}]^+$, the calculation confirms that (as expected) the SOMO is almost entirely (96%) on the dioxolene ligand, i.e., it is correct to call it a semiquinone (sq) species, and the low-energy, weak NIR transition at 1250 nm is an internal semiquinone-centered transition from a filled π orbital to the SOMO.[14] For a Ru(II)−sq complex in low symmetry it is expected that there can be three Ru[d(π)] $\rightarrow$ sq(SOMO) MLCT transitions, one from each of the ruthenium d(π) orbitals; the metal orbital which overlaps

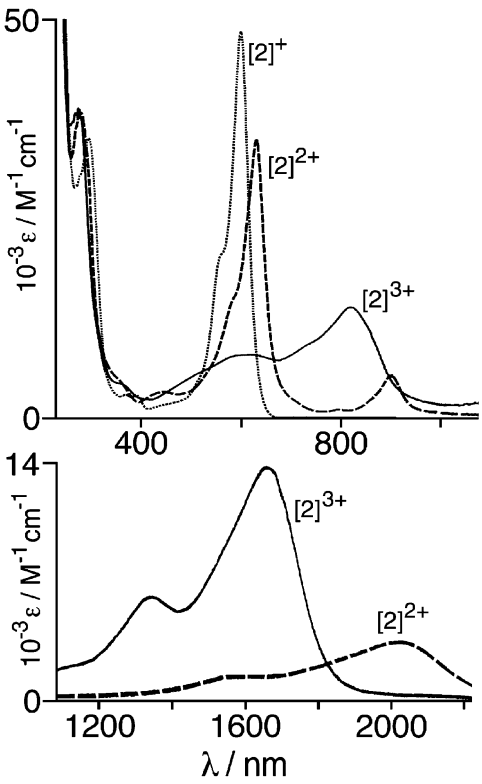

Figure 7. Electronic spectra of $[\mathbf{2}]^+$ (···) $[\mathbf{2}]^{2+}$ (- - -), and $[\mathbf{2}]^{3+}$ (—) recorded during an OTTLE experiment (CH_2Cl_2, 243 K).

most effectively with the sq π-system is expected to be the most intense and also to have the highest energy. The observed transitions at 582, 535, and 433 nm agree well with this assignment which is supported by the ZINDO calculation. At higher energy, the new 341 nm transition has a mixture of Ru $\rightarrow$ sq MLCT and sq-based $\pi \rightarrow \pi^*$ character, and the intense band at 283 nm consists of several components of which the most significant are sq-centered $\pi \rightarrow \pi^*$, and $PPh_3 \rightarrow$ sq ligand-to-ligand charge transfer.

(ii) Dinuclear Complex 2. The electronic spectra of $[\mathbf{2}]^+$ and its one-electron and two-electron oxidized forms $[\mathbf{2}]^{2+}$ and $[\mathbf{2}]^{3+}$ are in Figure 7 (see also Table 5). Most of the spectral assignments proposed below follow from the above analysis of **1**/$[\mathbf{1}]^+$ and are again based on ZINDO calculations, using the geometry provided by the crystal structure for $[\mathbf{2}]^+$. For the singly and doubly oxidized forms, the ZINDO calculations were performed on DFT-optimized geometries in which (for simplicity) the PPh_3 ligands were replaced by PMe_3.

In the fully reduced state $[\mathbf{2}]^+$ the electronic spectrum is dominated by an intense transition at 599 nm, which is analogous to the lowest-energy transition of **1** (Figure 6) in that it is mostly a ligand-centered $\pi \rightarrow \pi^*$ transition with a small amount of Ru[d(π)] $\rightarrow$ [bridging ligand (π^*)] MLCT character. On oxidation to $[\mathbf{2}]^{2+}$, two new features develop in the low-energy part of the spectrum: a relatively weak transition at 899 nm and a broad, much lower energy transition at ca. 2000 nm. The former of these does not have any strong counterpart in the computed spectrum, although the calculations do indicate a weak absorbance in this region ascribable to Ru[d(π)] $\rightarrow$ [bridging ligand(SOMO)] MLCT

(14) Haga, M.; Dodsworth, E. S.; Lever, A. B. P. *Inorg. Chem.* **1986**, *25*, 447.
(15) This footnote was deleted during revision.

transitions originating from the three inequivalent d(π) orbitals. The 2000 nm transition is an internal $\pi \rightarrow \pi^*$ transition (HOMO → SOMO) associated with the bridging ligand radical and is well reproduced by the calculation (the analogous transition in $[\mathbf{1}]^+$ occurred at ca.1300 nm). The main transition in the visible region, at 599 nm for $[\mathbf{2}]^+$, is reduced in intensity and slightly red-shifted to 626 nm, and is again largely bridging-ligand centered $\pi \rightarrow \pi^*$ in character. The higher-energy, weaker transitions around 400 nm for $[\mathbf{2}]^{2+}$ are also largely of bridging-ligand centered $\pi \rightarrow \pi^*$ character, originating from lower-energy filled π orbitals. According to the calculations no transitions in the UV or visible region for $[\mathbf{2}]^{2+}$ involve the PMe_3 or CO groups, but in the "real" complex (with axial PPh_3 ligands) mixing of frontier orbitals with the P-phenyl rings is likely, and this may account for some of the discrepancies, most notably the fact that the peak at 899 nm is not well reproduced in the calculations, being predicted to have a much lower intensity than it actually does.

On further oxidation to $[\mathbf{2}]^{3+}$, the two low-energy transitions are blue-shifted and become more intense (Figure 7). Attempts to match these transitions to calculated spectra were complicated by the fact that the calculation showed that the two lowest energy states are a singlet and a triplet, and that they are very close in energy, so the ground state could actually have triplet character with the doubly oxidized bridging ligand being a diradical. We could find no evidence for this in the EPR spectrum, with the EPR spectrum of $[\mathbf{2}]^{3+}$ being featureless, although such negative evidence is not conclusive. In view of this ambiguity we prefer not to attempt a detailed analysis of the spectra but just point out that, in view of the assignment of the spectrum of $[\mathbf{2}]^{2+}$, transitions of bridging-ligand centered $\pi \rightarrow \pi^*$ character and Ru[d(π)] → (bridging ligand) MLCT character are expected in this region.

(iii) Dinuclear Complex 3. The electronic spectra associated with oxidation of **3** to $[\mathbf{3}]^+$ and then $[\mathbf{3}]^{2+}$ are in Figure 8 (see also Table 5). The lowest-energy transition of **3** at 547 nm is directly analogous to the lowest-energy transitions of **1** and **2**, at 432 and 599 nm respectively; ZINDO calculations, based on a DFT-optimized geometry using axial PMe_3 ligands in place of PPh_3, showed that this has principally bridging-ligand based $\pi \rightarrow \pi^*$ character with a small amount of Ru[d(π)] → (bridging ligand) MLCT character. The two higher-energy transitions at 449 and 360 nm have similar provenance.

Oxidation to $[\mathbf{3}]^+$ results in appearance of two lower-energy transitions at 682 and 1118 nm, both being principally bridging-ligand based $\pi \rightarrow \pi^*$ transitions which, as in the spectra of $[\mathbf{1}]^+$ and $[\mathbf{2}]^{2+}$, have become red-shifted compared to the parent reduced complexes; a higher-energy series of transitions between 300 and 500 nm are also bridging-ligand based $\pi \rightarrow \pi^*$ transitions with some additional MLCT character involving the bridging ligand SOMO. In addition, a broad, intense transition appears at low energy in the spectrum of $[\mathbf{3}]^+$ at 2695 nm (3710 cm^{-1}; $\epsilon \approx 2 \times 10^4$ M^{-1} cm^{-1}). Such a feature is not present in any mononuclear complexes of this nature such as $[\mathbf{1}]^+$,[6] and has the

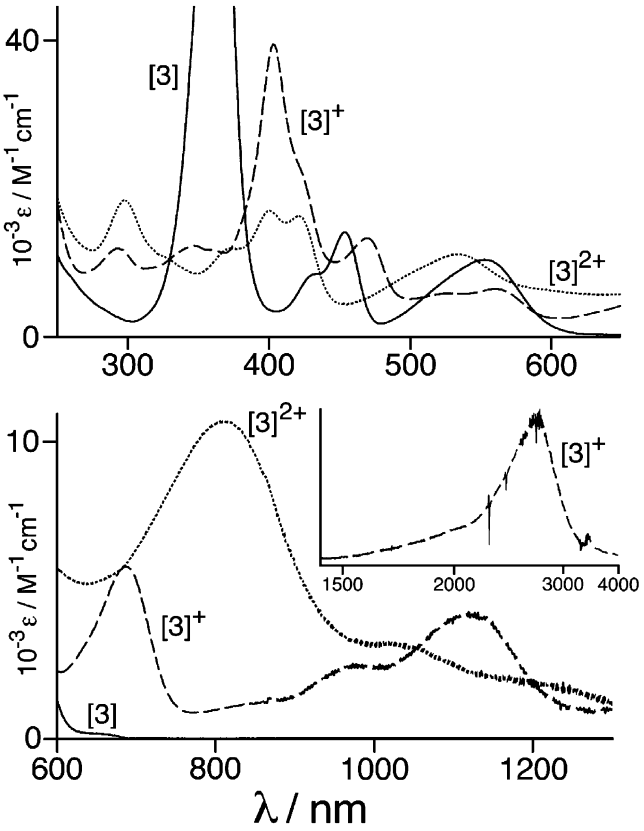

Figure 8. Electronic spectra of **3** (—), $[\mathbf{3}]^+$ (- - -), and $[\mathbf{3}]^{2+}$ (···) recorded during an OTTLE experiment (CH_2Cl_2, 243 K). The inset showing the IVCT transition for $[\mathbf{3}]^+$ is plotted in a linear energy scale.

characteristic position and appearance of an intervalence charge-transfer (IVCT) transition. This implies that the first oxidation of **3** is localized at one terminus of the bridging ligand, which can therefore be described has having distinct catecholate and semiquinone termini, i.e., a mixed-valence species; such a transition is consistent with a catecholate → semiquinone IVCT transition between the two termini of the bridging ligand.[16] The absorption is asymmetric, narrower on the low-energy side; this is most likely due to overlap of a narrow (width ca. 800 cm^{-1}) band near 3700 cm^{-1} with two weaker and broader (width ca. 2000 cm^{-1}) bands at higher energy.[18] The position of the absorption maximum is very slightly solvent-dependent, being blue-shifted in more polar solvents (THF, 3690 cm^{-1}; dichloromethane, 3710 cm^{-1}; acetone, 3800 cm^{-1}; acetonitrile, 3840 cm^{-1}), in keeping with its directional charge-transfer nature.

Meyer and co-workers have reviewed the class II to class III transition in mixed-valence complexes and have defined the new category class II−III.[17] The experimental criteria for class II−III mixed-valence compounds include the presence of narrow, solvent-independent, low-energy IVCT absorptions (typically associated with class III complexes),

(16) (a) Lahlil, K.; Moradpour, A.; Bowlas, C.; Nenou, F.; Cassoux, P.; Bonvoisin, J.; Launay, J.-P.; Dive, G.; Dahareng, D. *J. Am. Chem. Soc.* **1995**, *117*, 9995. (b) Lambert, C.; Nöll, G. *J. Am. Chem. Soc.* **1999**, *121*, 8434.

(17) Demandis, K. D.; Hartshorn, C. M.; Meyer, T. J. *Chem. Rev.* **2001**, *101*, 2655.

(18) This interpretation of the band at 3710 cm^{-1} was provided by Dr. Thomas J. Meyer (private communication).

combined with experimental evidence of localized (class II) electronic structure, such as the low symmetry of the CO stretches observed here. An IVCT transition at this energy for a class II mixed-valence state should be Gaussian and symmetric with a $\Delta\nu_{1/2}$ value of about 3000 cm^{-1} [from $\Delta\nu_{1/2} = (2310E_{op})^{1/2}$].

The narrowness and solvent-insensitivity of the IVCT band can be explained by solvent averaging, which requires that electron transfer be rapid compared to the rate of reorientation of local solvent dipoles (0.2−10 ps).[17] Accordingly the rate of electron transfer is greater than ca. 10^{11} s^{-1}, while still being slower than the IR time scale (10^{13} s^{-1}), which allows us to bracket the electron-transfer rate in a narrower range than we could get from comparison of the EPR and IR spectra (electron-transfer rate $> 10^8$ s^{-1} but $< 10^{13}$ s^{-1}). The behavior we see for $[\mathbf{3}]^+$ is therefore consistent with class II−III behavior as described by Meyer;[17] a more detailed analysis of the spectroscopic properties of $[\mathbf{3}]^+$ and related complexes will be the subject of further studies.

On further oxidation to $[\mathbf{3}]^{2+}$, the IVCT transitions and the 1118 nm ligand-centered transitions of $[\mathbf{3}]^+$ disappear (Figure 8) and are replaced by an intense transition at 810 nm. The ZINDO calculations on doubly oxidized $[\mathbf{3}]^{2+}$ highlight the same problem that occurs for calculations of $[\mathbf{2}]^{3+}$, viz., that there are singlet and triplet states very close in energy such that the ground state could be either. Actually the triplet ground state gives a much better prediction of the observed electronic spectrum than does the singlet state; both confirm the presence of a near-IR transition at ca. 1000 nm, having a mixture of bridging-ligand centered $\pi \rightarrow \pi^*$ and some MLCT character, but if the ground state is assumed to be a singlet the predicted intensity of this transition is enormously over-estimated. The predicted triplet spectrum in contrast gives a reasonable intensity for this transition. Given the ambiguity in the nature of the ground state, further analysis of this spectrum is inappropriate.

Conclusions

Mononuclear complex **1** and dinuclear complexes $[\mathbf{2}]^+$ and **3** undergo reversible oxidations (one for **1**, two each for **2** and **3**) which are formally catecholate/semiquinone-type processes associated with the dioxolene bridging ligands. For **3**, the separation between the two successive processes (440 mV) is substantially less than in $[\mathbf{2}]^+$ (690 mV), indicative of a weaker electronic coupling—and hence less delocalization in the mixed-valence state—for **3** compared to $[\mathbf{2}]^+$. For these dinuclear complexes, mono-oxidation generates a ligand-centered "mixed-valence" radical for which the extent of delocalization could be studied by IR and EPR spectroscopy. EPR spectra indicate that both $[\mathbf{2}]^{2+}$ and $[\mathbf{3}]^+$ are delocalized on the EPR time scale; however IR spectra indicate that whereas $[\mathbf{2}]^{2+}$ is also delocalized on the IR time scale at 243 K, $[\mathbf{3}]^+$ is localized with spectroscopically distinct $\{Ru(CO)_2\}$ termini, with evidence for coupling between the two pairs of CO vibrations. Accordingly the rate of exchange of the odd electron between the two termini of $[\mathbf{3}]^+$ can be bracketed, as greater than 10^8 s^{-1} (EPR time scale) but less than 10^{13} s^{-1} (IR time scale) at 243 K. UV/vis/NIR spectroelectrochemical experiments were performed to measure the electronic spectra of these complexes in all accessible oxidation states; these spectra were partially assigned with the aid of ZINDO calculations. Mixed-valence complex $[\mathbf{3}]^+$ shows a low-energy transition in its electronic spectrum ascribable to a catecholate → semiquinone intervalence charge transfer between inequivalent termini (cf. the IR spectra data); the narrowness of the IVCT band indicates solvent averaging and suggests that the electron-transfer rate is actually greater than 10^{11} s^{-1} (borderline class II−III behavior). No such transition is present for $[\mathbf{2}]^{2+}$. These results are in agreement with the smaller separation between the two redox processes of **3** compared to $[\mathbf{2}]^+$.

Experimental Section

General Details. The ligands H_2L^1 and H_3L^2 were purchased from Aldrich and used as received; rufigallol (H_4L^3) was prepared according to a literature procedure.[19] $Ru_3(CO)_{12}$ was obtained from Strem.

Physical and Spectroscopic Methods. UV/vis/NIR spectroelectrochemical measurements were performed in a home-built OTTLE cell mounted in the sample compartment of a Perkin-Elmer Lambda 19 spectrometer as described previously;[20] distilled CH_2Cl_2 was the solvent in every case, and all measurements were carried out at −30°C (to minimize evaporation of the solvent from the cuvette during the experiment). For all of the transformations described, clean isosbestic points were obtained and the spectra of the starting materials could be regenerated with no significant changes by reversing the electrolysis. IR spectroelectrochemical measurements were carried out using a homebuilt OTTLE cell based on a KBr microcavity cuvette (Spectratech), with a Pt-gauze working electrode, a Pt wire counter electrode, and an Ag wire coated with AgCl as the reference; again, distilled CH_2Cl_2 was used as solvent and the measurements were carried out at −30 °C using a Bruker IFS-25 spectrometer. Electrochemical measurements were carried out as described previously, using a standard three-electrode cell;[5] ferrocene was used as an internal standard, and all potentials are quoted vs the ferrocenium/ferrocene couple. X-band EPR spectra were recorded on either an IBM/Bruker ER-200 SRC spectrometer (Buffalo) or a Bruker ESP-300E spectrometer (Bristol), in CH_2Cl_2 solutions at room temperature using a microwave power of 20 mW; spectral parameters were determined by comparison of experimental spectra with spectra simulated using Bruker WINEPR Simfonia (ver. 1.25) software. Other instrumentation used for routine measurements on **1** and $[\mathbf{2}][PF_6]$ carried out in Bristol have been described before.[5] Measurements on complex **3** at Buffalo used the following equipment: infrared spectra, a Nicolet Magna 550 spectrophotometer; NMR spectra (in $CDCl_3$), Varian Associates Gemini 300 or VXR-400S instruments; UV/visible spectra (300−800 nm), a Hewlett-Packard 8452A diode array spectrophotometer.

Syntheses. (a) $[Ru(CO)_2(PPh_3)_2(L^1)]$, 1. A mixture of $Ru_3(CO)_{12}$ (140 mg, 0.22 mmol), PPh_3 (380 mg, 1.46 mmol), and H_2L^1 (140 mg, 0.71 mmol) in dry toluene (30 cm^3) under N_2 was heated to reflux for 12 h to give a red solution. After removal of the solvent in vacuo, the crude material was purified by column chromatography (alumina, CH_2Cl_2:MeOH, 99:1 v/v). The second (major) orange band was the product: yield, 0.302 g (52%). FABMS: *m*/*z* 888 (M^+), 860 ($M^+ - CO$), 626 ($M^+ - PPh_3$). $^{31}P\{^1H\}$ NMR: δ

(19) Grimshaw, J.; Haworth, R. D. *J. Chem. Soc.* **1956**, 4224.
(20) Lee, S.-M.; Kowallick, R.; Marcaccio, M.; McCleverty, J. A.; Ward, M. D. *J. Chem. Soc., Dalton Trans.* **1998**, 3443.

17.0 (PPh_3). IR (CH_2Cl_2): 2042, 1978, 1686 cm^{-1}. Anal. Calcd for $C_{48}H_{36}O_7P_2Ru$: C, 64.9; H, 4.1. Found: C, 64.5; H, 4.0.

(b) [{Ru(CO)$_2$(PPh$_3$)$_2$}$_2$(L^2)][PF$_6$], (2)[PF$_6$]. A mixture of $Ru_3(CO)_{12}$ (100 mg, 0.16 mmol), PPh_3 (380 mg, 1.45 mmol), and H_3L^2 (120 mg, 0.357 mmol) in dry toluene (30 cm^3) under N_2 was heated to reflux for 15 h to give a deep blue solution. After removal of the solvent, the crude material was purified by column chromatography (alumina, CH_2Cl_2: MeOH, 95:5 v/v). After removal of traces of unreacted $Ru_3(CO)_{12}$, a deep blue band eluted, which was collected and evaporated to dryness. The blue complex was redissolved in the minimum amount of MeOH and precipitated as its hexafluorophosphate salt by addition of aqueous KPF_6. The suspension was extracted several times with CH_2Cl_2; the combined organic extracts were dried over $MgSO_4$ and evaporated to dryness to give pure (**2**)[PF_6], which was finally recrystallized from CH_2Cl_2/hexanes. Yield: 0.309 g (45%). FABMS: *m*/*z* 1680 (M − PF_6)$^+$, 1417 (M − PF_6 − PPh_3)$^+$, 1391 (M − PF_6 − PPh_3 − CO)$^+$, 1157 (M − PF_6 − 2PPh_3)$^+$. $^{31}P\{^1H\}$ NMR: δ 21.3 (PPh_3), −144.2 (septet, PF_6^-). IR (CH_2Cl_2): 2046, 1988, 1607 cm^{-1}. Anal. Calcd for $C_{95}H_{69}F_6O_9P_5Ru_2 \cdot CH_2Cl_2$: C, 60.3; H, 3.7. Found: C, 60.1; H, 3.7.

(c) [{Ru(CO)$_2$(PBu$_3$)$_2$}$_2$(L^3)], 3. A solution of $Ru_3(CO)_{12}$ (104 mg, 0.162 mmol), PBu_3 (240 μL, 0.95 mmol), and rufigallol (81 mg, 0.27 mmol) in dry toluene (20 cm^3) was heated at reflux under an argon atmosphere for 7 h. The resulting red solution was evaporated to dryness, and the residue was applied as a dichloromethane solution to a silica gel preparative TLC plate. Elution with 4% ethyl acetate in dichloromethane gave a red-brown colored band, which was extracted with ethyl acetate. Recrystallization from methanol gave brown crystals. Yield: 212 mg, 61%. ^1H NMR ($CDCl_3$): δ 13.15 (s, 2 H), 7.02 (s, 2 H), 1.74 (m, 12 H), 1.46 (br, 12 H), 1.38 (m, 12 H), 0.90 (t, 18 H, *J* 7 Hz). $^{13}C\{^1H\}$ NMR ($CDCl_3$): 197.9 (br t, 4 C, J_{PC} 11 Hz), 186.9 (2 C), 167.1 (2 C), 154.6 (2 C), 153.8 (2 C), 123.6 (2 C), 110.1 (2 C), 110.0 (2 C), 25.6 (12 C), 24.6 (t, 12 C, J_{PC} 6 Hz), 22.9 (t, 12 C, J_{PC} 12 Hz), 13.9 (12 C) ppm. $^{31}P\{^1H\}$ NMR ($CDCl_3$): δ 19.11 (PBu_3). IR (CH_2Cl_2): 2030 vs, 1965 s cm^{-1}. Anal. Calcd for $C_{66}H_{112}O_{12}P_4Ru_2$: C, 55.7; H, 7.9. Found: C, 55.7; H, 8.0.

Crystallography. Suitable crystals were mounted on a Bruker SMART-CCD (for **1**) or APEX (for [**2**][PF_6]·3CH_2Cl_2) diffractometer equipped with graphite-monochromatized Mo Kα radiation. Crystallographic measurements were carried out at 173 K (for **1**) or 100 K (for [**2**][PF_6]·3CH_2Cl_2); details of the crystal, data collection, and refinement parameters are summarized in Table 1, and selected structural parameters are collected in Tables 2 and 3. After integration of the raw data and merging of equivalent reflections, an empirical absorption correction was applied based on comparison of multiple symmetry-equivalent measurements.[21] The structures were solved by direct methods and refined by full-matrix least squares on weighted F^2 values for all reflections using the SHELX suite of programs.[22] All non-hydrogen atoms were assigned anisotropic displacement parameters (apart for a few disordered atoms in the structure of [**2**][PF_6]·3CH_2Cl_2, see below) and refined without positional constraints; hydrogen atoms were constrained to ideal geometries and refined with fixed isotropic displacement parameters. For **1** the solution and refinement were straightforward and presented no problems. The structural determination of [**2**][PF_6]·3CH_2Cl_2 was complicated by the presence of disorder involving the bridging ligand and some of the solvent molecules. In the picture shown in Figure 2, the phenyl substituent of the bridging ligand [C(141)−C(146)] is directed into the page and the central oxygen atom O(21) is at the front, with a lattice CH_2Cl_2 molecule nearby; the disorder involves all of these components swapping over such that the region either side of the center of the bridging ligand is occupied by a partial phenyl ring and a partial CH_2Cl_2 molecule. Atoms O(21) and C(14) were likewise mutually disordered. This could be successfully resolved, but the disordered C atoms had to be refined with isotropic thermal parameters; H atoms were not included on these C atoms.

Calculations. The INDO/S-derived predicted spectra and molecular orbital descriptions were based on DFT optimized structures and will be discussed in depth elsewhere.[23] These data were obtained using the INDO/S method in the HYPERCHEM 5.1 program (Hypercube Inc., Gainesville, FL). The DFT calculations presented were carried out using the GAUSSIAN 98 program[24] using Becke's three-parameter hybrid functional[25] with the LYP correlation functional[26] (B3LYP) and an effective core potential basis set LanL2DZ.[27] For further details see ref 28.

Acknowledgment. Financial support from EPSRC and Johnson Matthey (U.K.) is gratefully acknowledged. We thank Dr. Thomas J. Meyer of Los Alamos National Laboratory for helpful comments concerning the spectroscopy of the mixed-valence species [**3**]$^+$, and Dr. John Maher of the University of Bristol for assistance with the EPR spectroscopy.

Supporting Information Available: Crystallographic data in CIF format. This material is available free of charge via the Internet at http://pubs.acs.org.

IC034579O

(21) Sheldrick, G. M. *SADABS*: *A program for absorption correction with the Siemens SMART system*; University of Gottingen: Göttingen, Germany, 1996.
(22) *SHELXTL program system*, version 5.1; Bruker Analytical X-ray Instruments Inc.: Madison, WI, 1998.
(23) Lever, A. B. P.; Keister, J. B.; Ward, M. D., in preparation.
(24) Frisch, M. J.; Trucks, G. W.; Schlegel, H. B.; Scuseria, G. E.; Robb, M. A.; Cheeseman, J. R.; Zakrzewski, V. G.; Montgomery, J. A., Jr.; Stratmann, R. E.; Burant, J. C.; Dapprich, S.; Millam, J. M.; Daniels, A. D.; Kudin, K. N.; Strain, M. C.; Farkas, O.; Tomasi, J.; Barone, V.; Cossi, M.; Cammi, R.; Mennucci, B.; Pomelli, C.; Adamo, C.; Clifford, S.; Ochterski, J.; Petersson, G. A.; Ayala, P. Y.; Cui, Q.; Morokuma, K.; Malick, D. K.; Rabuck, A. D.; Raghavachari, K.; Foresman, J. B.; Cioslowski, J.; Ortiz, J. V.; Stefanov, B. B.; Liu, G.; Liashenko, A.; Piskorz, P.; Komaromi, I.; Gomperts, R.; Martin, R. L.; Fox, D. J.; Keith, T.; Al-Laham, M. A.; Peng, C. Y.; Nanayakkara, A.; Gonzalez, C.; Challacombe, M.; Gill, P. M. W.; Johnson, B.; Chen, W.; Wong, M. W.; Andres, J. L.; Gonzalez, C.; Head-Gordon, M.; Replogle, E. S.; Pople, J. A. *GAUSSIAN-98*, revision A.7; Gaussian Inc.: Pittsburgh, PA, 1998.
(25) Becke, A. D. *J. Chem. Phys.* **1993**, *98*, 5648.
(26) Lee, C.; Yang, W.; Parr, R. G. *Phys. Rev. B* **1988**, *37*, 785.
(27) (a) Dunning, T. H., Jr.; Hay, P. J. In *Modern Theoretical Chemistry*; Schaefer, H. F., III, Ed.; Plenum: New York, 1976; Vol. 3, p 1. (b) Hay, P. J.; Wadt, W. R. *J. Chem. Phys.* **1985**, *82*, 270. (c) Hay, P. J.; Wadt, W. R. *J. Chem. Phys.* **1985**, *82*, 284. (d) Hay, P. J.; Wadt, W. R. *J. Chem. Phys.* **1985**, *82*, 299.
(28) Gorelski, S. I.; Lever, A. B. P.; Ebadi, M. *Coord. Chem. Rev.* **2002**, *230*, 97.